Automated Robotics Peeling Platform for the Interfacial Adhesion Characterization of Micro-scale Free Elementary Bio-based Fibers

Wajih Akleh[1], Jason Govilas[1], Thomas Guibaud[1], Vincent Placet[1], Cédric Clévy[1,a]

***Abstract*—This article focuses on the development of an experimental platform capable of performing, to the authors' knowledge, for the first time, peeling tests on bio-based fibers. These fibers are very small, their diameters being no larger than a few tens of micrometers, and are not attached to a substrate. The interfacial adhesion forces between elementary fibers have not been quantified and also require quite large motions (mm). To address these challenges, a micro-robotics approach is investigated that combines a micro-gripper, two micro-force sensors, a reduced friction guidance system, and two synchronized micro-positioning stages. This paper presents the operating principle of the robotic platform, its calibration, its measurement protocol and automated experimental tests that quantify, for the first time, the typical magnitude of peeling forces that is of the order of $10\,mN$, resulting in an interfacial adhesion of $0.26 \pm 0.13\,mN/mm$. Several experimental tests are conducted on hemp and nettle fibers proving the versatility of the approach. These works also establish a correlation between the microstructure of the fibers and their adhesion strength, opening up to further mechanical analysis of the adhesion mechanisms of plant fibers which are highly interesting for the development of bio-based composites and for the investigation of bio-mimetic principles.**

***Index Terms*—Automation at Micro-Nano Scales; Micro/Nano Robots; Engineering for Robotic Systems**

I. INTRODUCTION

OVER the past few decades, the interest in bio-based fibers has increased drastically in a variety of fields [1], [2] due to their potential contribution in bio-inspired adhesives, and their sustainability and environmental impact in bio-composite applications compared to conventional composites [3]. For this type of application, it is crucial for plant fibers to be properly extracted and separated from the bundles in which they are naturally organized. Bio-based fibers, such as hemp, nettle, and flax are microscale objects with a diameter no larger than a few tens of micrometers, and a length of few millimeters. They have a complex internal structure that includes walls, lumen, fibrils, kink bands, etc. The quantification of interfacial adhesion between bio-based fibers appears to be of key interest. However, to the best of the authors' knowledge, there exists no data or experimental devices capable of quantifying such adhesion.

In this scope, peel-type tests appear promising. For example, ISO 11339:2022 and ASTM-D1876 refer to the widespread T-Peel test to quantify the resistance of adhesive and flexible-to-flexible bonded assemblies. While many experimental platforms have been developed and allow peeling tests to be carried out, they address the peeling of films, typically adhesives, and concern surfaces of macro-metric dimensions, i.e. the dimensions of which are greater than several millimeters. The study of peeling at small scales, i.e. millimeter and below, currently constitutes a particularly important and promising field of investigation. If various existing works explore the modeling of small-scale phenomena, their experimental validation constitutes a major obstacle [4]. Indeed, carrying out peeling tests on Y-shaped natural fibers requires a system for fixing two ends (the fibers being "free" objects, not fixed to a substrate), generating a pretension between them, grasping the third end and then pulling it in a desired direction while controlling the speed and measuring the pretension and peeling forces, as is illustrated in Fig. 1.a and b. All of these systems must be adapted not only to the dimensions of the fibers but also to the orders of magnitude of the forces to be applied and the displacements to be generated. The main objective of this article is to develop an experimental platform capable of carrying out this type of test and determining, for the first time, the orders of magnitude of interfacial adhesion for bio-based fibers.

In the field of adhesives, the development of experimental tests on small-sized films has been investigated, where this difficulty of integrating several systems in a reduced volume adapted to small objects has been addressed by new principles for carrying out peel tests. For example, Petterson et al. [5] have developed a principle of peeling a film wrapped around a rotating cylinder which guarantees their perpendicularity during the tests. This work deals with films of $2\,mm$ in width and $185\ \mu m$ thick and enables to apply a peeling force of $400\ mN$. Badler et al. [6] have customized a tribometer by making two coaxial rotating disks, one of which is made up of matrices of small pads having a diameter of $300\ \mu m$. The

Manuscript received: January 23, 2025; Revised May 5, 2025; Accepted November 16, 2025.

This paper was recommended for publication by Editor Xinyu Liu upon evaluation of the Associate Editor and Reviewers' comments. This work was supported by the European Union's Horizon 2020 research and innovation program under grant agreement No. 771134. The project NETFIB was carried out under the ERA-NET Cofund SusCrop (Grant No. 771134), being part of the Joint Programming Initiative on Agriculture, Food Security and Climate Change (FACCE-JPI). This work has also been supported by EIPHI Graduate School under grant agreement "ANR-17-EURE-0002", the ANR Dynabot (contract "ANR-21-CE10-0016") and the French RENATECH and ROBOTEX networks (TIRREX ANR-21-ESRE-0015) through their FEMTO-ST technological facilities MIMENTO and CMNR.

[1]Authors are with Université Marie et Louis Pasteur, SUPMICROTECH, CNRS, Institut FEMTO-ST, F-25000 Besançon, France. [a]IEEE Senior Member. wajih.akleh@femto-st.fr, cedric.clevy@femto-st.fr

Digital Object Identifier (DOI): see top of this page.

rotation of one disk relative to the second allows peeling to be carried out off the surface of the pads, where peeling forces of $800mN$ are thus generated. These works are dedicated to films and the dimensions of the objects considered are an order of magnitude larger than the diameters of bio-based fibers. The applicability of such approaches to performing peel tests on natural fibers therefore does not appear feasible.

In the field of AFM (Atomic Force Microscopy), some works show a possibility to achieve tasks other than topography [7]. Schmied et al. [8] have notably used AFM cantilevers (with a tip) to compress bio-based fibers, and succeeded in measuring orders of magnitude of detachment forces of "single fibrils" for natural cellulosic fibers (around 20 μN), "fibril bundles" (around $65\mu N$), and "cell wall delamination" (around 95 μN) which are elementary sub-parts of bio-based fibers. Movements of approximately $10\,\mu m$ are generated and forces between 100 and 600 μN have been measured. Approaches based on AFM are not directly applicable to achieve peeling tests at the level of bio-based fibers where several issues should be solved such as the way to attach a tip of the fiber to the AFM cantilever, designing specific AFM cantilever to achieve strong enough peeling forces, and generating motions much larger than few micrometers.

The field of tethered micro-robotics has been under active development and enables the dense integration of several systems. Some key recent results include the creation of very small structures with large motion capabilities [9], [10], the integration of on-board micro-force sensors [11], [12], [13], and the carrying out of precise robotic tasks on the micrometric scale [14], [15], [16], [17] which requires control of forces typically from a few tens to hundreds of μN [18], [19]. This approach allows for peeling tasks on non-planar (spherical) substrates, particularly in the field of retinal surgery [20]. Measurement of forces beyond human dexterity i.e. a few mN [21], and the compensation for the tremors of the human operator in a surgeon-robot collaboration approach [22] have been investigated. This micro-robotic approach has also been implemented to study the properties of single bio-based fibers using grippers mounted on micro-robotic structure. The bonding of one end of the fiber to a force sensor and the use of micro-gripper enabled tensile testing, lateral deformation or inter-fiber joint strength tests of paper-making fibers. These pioneering works demonstrate displacements of a few tens of micrometers, with forces typically measured at the 10 mN scale [23], [24] allowing for comparative studies of several batches of fibers in a qualitative way [25], [26].

Micro-robotic tools and methods thus appear promising to design an experimental platform able to perform peeling tests on bio-based fibers. This platform combines a micro-gripper, two micro-force sensors, a reduced friction guidance system, and two synchronized micro-positioning stages. This paper presents the operating principle of the robotic platform, its calibration, its measurement protocol and automated experimental tests.

Thus, section II-A will introduce elements relating to elementary bio-based fibers, their structural complexity (Fig. 2) and their interest, section II-B the typical models of peeling tests and their key parameters. Section II-C will describe the operating principle of the experimental platform proposed. Sections II-D and II-E will respectively introduce the platform calibration principle as well as the proposed experimental protocol. Section III presents the main experimental results useful for validating the proposed approach and notably includes typical curves and the first orders of magnitude obtained for the peeling of free bio-based fibers. Section IV concludes the paper.

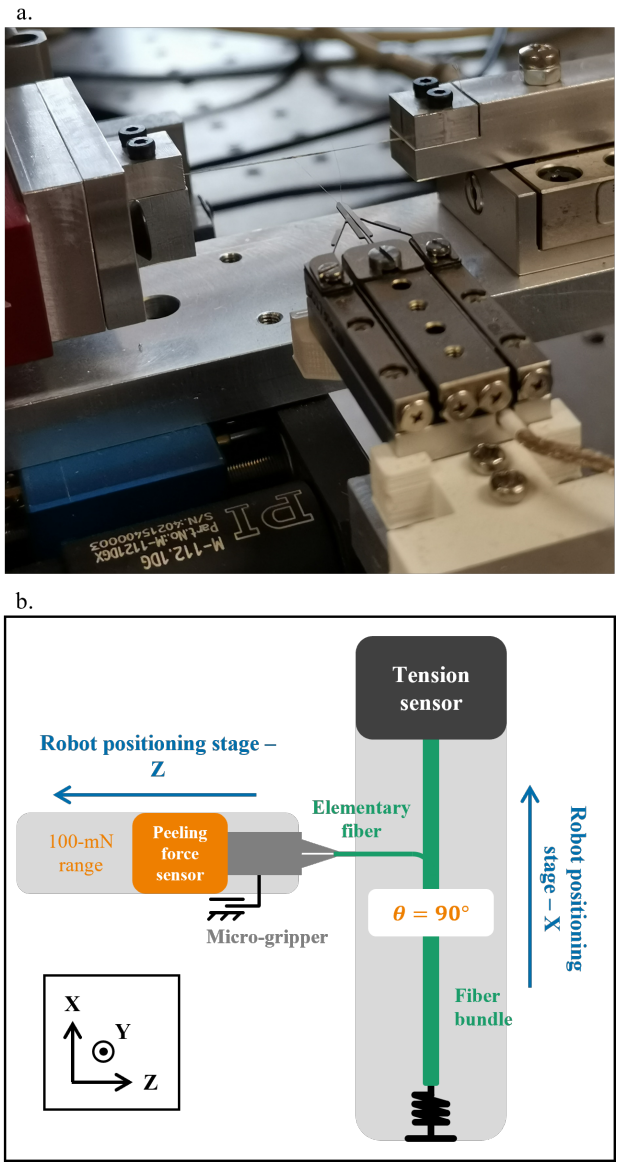

Fig. 1. Plant fiber mounted in the jaws of the peeling platform (a.) with a detailed schematic illustration of the peeling principle (b.).

II. MATERIALS & METHODS

A. Plant fibers

On the micro-structural level, plant fibers present a complex morphology with a primary outer wall and a secondary wall composed of three layers [27], and two main morphological particularities that are highlighted in Fig. 2 - kink-bands and cellulose micro-fibrils. A kink-band is a point along the length

of the elementary fiber where the micro-structure of the fiber undergoes a significant change and leads to the formation of nodes or dislocation bands [28].

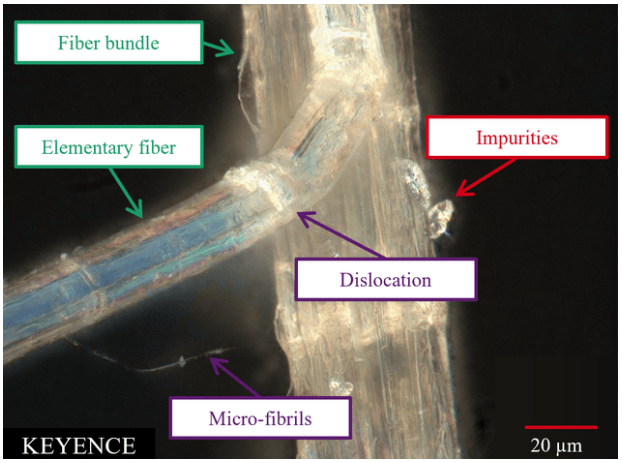

Fig. 2. Microscopic image of a peeled plant fiber.

Plant fiber quality and the interfacial adhesion of plant fibers are susceptible to a number of parameters relating to their intricate interfacial structure, their morphological complexity, and their transformation process [29]. Therefore, the characterization of this force represents a point of interest for the extension of the accumulated knowledge on plant fibers and the development of more reliable and accurate ways to control fiber quality for the various growing applications.

Being one of the top cultivated bast fibers in Europe during the last few decades, and due to their high versatility in various applications, hemp fibers of the species Futura 75 and nettle fibers constitute the object of study of this work.

Prior to peeling tests, fiber bundles are manually extracted from the provided strands and cut to a length suitable for mounting on the peeling setup. Once a bundle is extracted, an elementary fiber is partially manually separated from it under a magnifying lens. The elementary fiber is not fully detached from its parent bundle but rather peeled until an adequate portion of around $10\,mm$ is protruding, which can be easily grasped by a micro-gripper to initiate the peeling.

B. Peeling model

Peeling models allow the calculation of an adhesion constant specific to the tested material, taking into account the geometrical properties of the peeled object, and can ultimately be used to compare the interfacial adhesion of different materials.

The Kendall model is a general representative model for thin-film peeling that allows the determination of the adhesion constant E between a peeled thin elastic film and a rigid substrate based on this following equation in the case of large peel angles [30]:

$$E = \frac{F \times (1 - \cos\theta)}{b} \tag{1}$$

The adhesion constant is denoted E and is calculated from the peeling force F, applied at an angle θ, necessary to separate a thin film of width b from a peeling substrate as shown in Fig. 3.a [30]. This formulation is valid for large peeling angles of over $45°$.

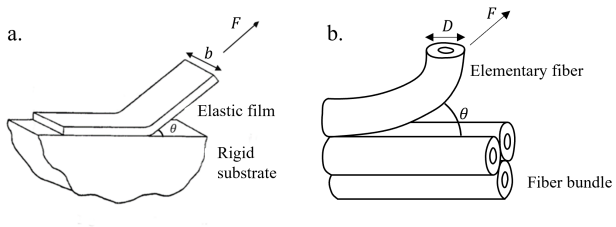

Fig. 3. Illustration of the Kendall thin-film peeling model [30] (a.) and the equivalent plant fiber peeling model considered in this work (b.).

This model is adjusted to plant fiber peeling by replacing the thickness term b by the diameter of the peeled fiber D which is considered perfectly cylindrical, giving the modified equation 2 for the adhesion constant calculated for plant fibers. Fig. 3.b illustrates the similarity between the Kendall thin-film peeling model and the proposed plant fiber peeling model. The peeled fiber diameter D is a first estimation of the contact width between the peeled fiber and its parent bundle. This model does not reflect the morphological complexity of the fiber itself or its interface with other fibers within the bundle. However, a precise calculation of the contact surface between the peeled fiber and its bundle throughout the peeling test represents a significant vision problem considering the complexity of the object and the sample movement during the test. This approach thus presents a simpler approximation of the contact width, it being the apparent diameter of peeled elementary fiber as observed in-situ, which allows for comparative studies between samples.

$$E = \frac{F \times (1 - \cos\theta)}{D} \tag{2}$$

C. Experimental platform

The experimental setup, as shown in Fig. 4, is designed for micro-scale fiber-peeling operations and relies on a set of linear actuators [PI, M-111· M-112 Compact Micro-Translation Stage], force sensors [peeling force sensor: TEI, FSB101, and pretension sensor: AEP Transducers®, TCA, CTCA1K5], and a micro-gripper [SmarAct, SG-1730 - Micro-Gripper] to achieve precise and synchronized manipulation of the target fiber at the micrometer level.

Determining an adhesion constant for plant fibers requires knowledge of the following three quantities: the peeling force F, the peeling angle θ, and the fiber diameter D. The setup also is designed to enable a peeling angle of $90°$ to be maintained during the entire peeling test and for a controlled tension to be applied on the fiber bundle, both factors being essential for the proper application of the peeling model.

A fiber bundle is fixed and visually centered between screw-secured jaws along the x-axis, with a single elementary fiber extending from it along the z-axis. One of the jaws has a rotating head that enables the fiber to be properly oriented

facing the micro-gripper without twisting the bundle. The fiber bundle tension between the jaws is applied and adjusted using a manual micro-positioning stage to minimize the deflection of the fiber bundle during peeling, ensuring a rigid peeling substrate. The micro-gripper clamps the elementary fiber, and the gripper actuator retreats along the z-direction, exerting force to peel the fiber off from its parent bundle. Two larger manual XYZ tables allow the positioning of the bundle and micro-gripper parts of the setup relative to each other.

In order to measure the peeling force exerted by the micro-gripper, a connection with the peeling force sensor that inhibits a rigid body interaction is necessary. For this reason the micro-gripper is placed on a custom 3D printed support, mounted on a IKO slider rail system on one hand and to the force sensor on the other. This configuration offers a degree of freedom to the micro-gripper, with respect to the force sensor, allowing for a relative, low friction, linear displacement between the two components along the z-axis. In this way their independent operation and thus the accurate measurement of the peeling force is guaranteed.

The fiber-bundle adhesion constant is determined as per the aforementioned Kendall model, Eq. 2, based on the force measured in this peeling action. This force is measured during the peeling test by the peeling force sensor that is located behind the micro-gripper.

The second term in the adhesion equation is the peeling angle. To eliminate the need for a continuous measurement of the peeling angle during the test and to contribute to higher repeatability and consistency between tests, a constant peeling angle is desired. For this purpose, an actuator is used at the bundle level on the x-axis and moves in synchronization with the micro-gripper actuator in the opposite direction to that of the peeling propagation, maintaining a constant peeling angle throughout the peeling test. Thus, the simplified Kendall's hypothesis is satisfied and the $\cos\theta$ term is taken out of the equation.

Fig. 5 shows an illustration of a mounted bundle with its elementary fiber grasped by the micro-gripper, highlighting the motion of the actuators during the peeling action.

In addition to maintaining a constant peeling angle, the second linear actuator plays an important role in the observation of the peeling process during the tests. A telecentric camera, mounted above the sample on the setup and positioned above the peeling zone, provides a visual output of the area of interest. The telecentric lens provides constant magnification and a high depth of field without distorting the observed fiber in order to measure its apparent diameter. The synchronized movement of the two actuators allows for the peeling zone to stay inside the frame of vision of the camera during the test.

The different electronic components of the experimental platform are controlled via Simulink allowing automated control and execution of the peeling operations according to specified input parameters (peeling speed and distance). The block diagram shown in Fig. 5 summarizes the mode of operation of the experimental platform.

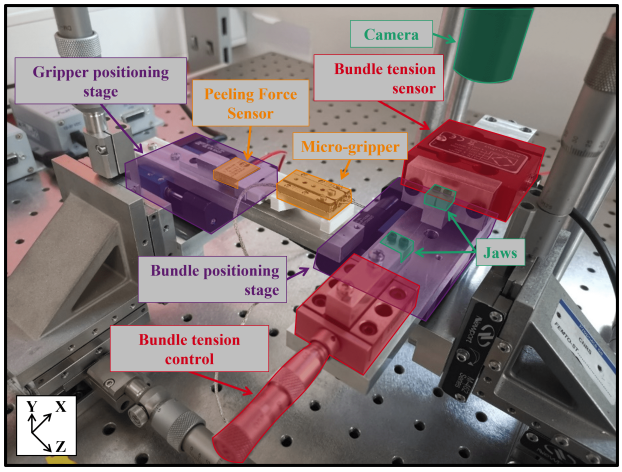

Fig. 4. Experimental setup for plant fiber peeling with the main components highlighted: the jaws used for gripping the fiber bundle, the bundle tension sensor and its control stage, the two positioning actuators which ensure the synchronized movement of the bundle (x-axis) and the micro-gripper (z-axis) that is connected to the peeling force sensor. The camera provides footage in real time of the peeling (camera view shown in the bottom right corner).

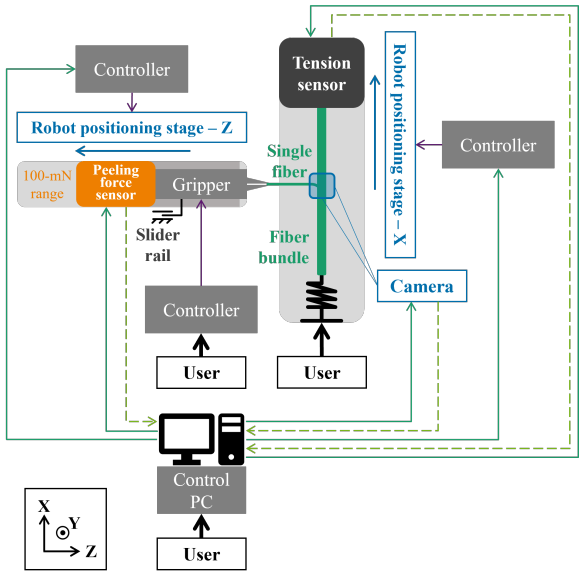

Fig. 5. Experimental platform block diagram showing the communication between the different components of the setup: thick black arrows represent user input (test parameters), thin black and dark green arrows component control, light green component output (collected test data), and dark blue arrows movement direction during peeling.

D. Peeling test calibration

With the implementation of the rail system at the micro-gripper-peeling-force-sensor level, and due to the inertia of the different components, the peeling force sensor output data would consist of not only the measured peeling force required to separate the plant fibers, but also the friction forces that are present during the micro-gripper movements. To obtain the force related to the peeling of the fiber, the frictional forces must thus be characterized through a calibration process and subtracted from the total force as follows:

$$F_{peeling} = F_{measured} - F_{correction} \tag{3}$$

The calibration is performed by moving the micro-gripper, without any samples on the setup, backwards and forwards along the z-axis, in the direction of peeling and returning to the initial position, respectively, at various speeds over 5 repetitions. The retreating motion occurs at low speeds over the adopted peeling distance of $5\,mm$.

With the goal of performing the peeling tests at a low quasi-static speed of $0.001\ mm/s$ to minimize the effect of time-dependent phenomena on the observed peeling behavior, the calibration is repeated with a total of 25 speeds within the range of $0.001 - 0.100\ mm/s$; with a convergence of the measured force as a function of the distance traveled at a certain relatively high speed, a calibration test could be performed before each peeling test, providing thus a test-specific correction.

As seen in Fig. 6, the average standard deviation of the force, measured by the peeling force sensor along the z-axis, calculated for the 5 repetitions at a single speed does not exceed $10^{-4}\,N$ for any tested speed, which corresponds to the peeling force sensor noise, indicating good repeatability of the peeling force sensor output. Fig. 6 highlights two calibration tests at speeds of 30 and 71 $\mu m/s$, with the 5 repetitions at each speeds; only a single repetition is shown in color for ease of reading the plot. The superposition of the 5 curves indicates high repeatability of the measurements at one speed, with a standard deviation of the 5 being lower than $10^{-4}\,N$ when the measured forces are of the order of $10^{-1}\,N$.

However, regarding the linear fit of the obtained data for each tested speed, the linear slope presents a significant difference of 3.5% between its value at the standard peeling speed ($0.001mm/s$) and the next tested speed ($0.0051mm/s$). Therefore, the correction to be applied to the peeling force must be extracted at the standard peeling speed, thus preventing the possibility of running a calibration for each individual peeling test.

As a result of this calibration campaign, a single calibration test is performed over a $5\,mm$ distance along the z-axis at a speed of $0.001mm/s$ and its output is applied as a quadratic fit correction for the peeling force for the entire testing campaign for an expected high precision of the measured force within the sensor noise.

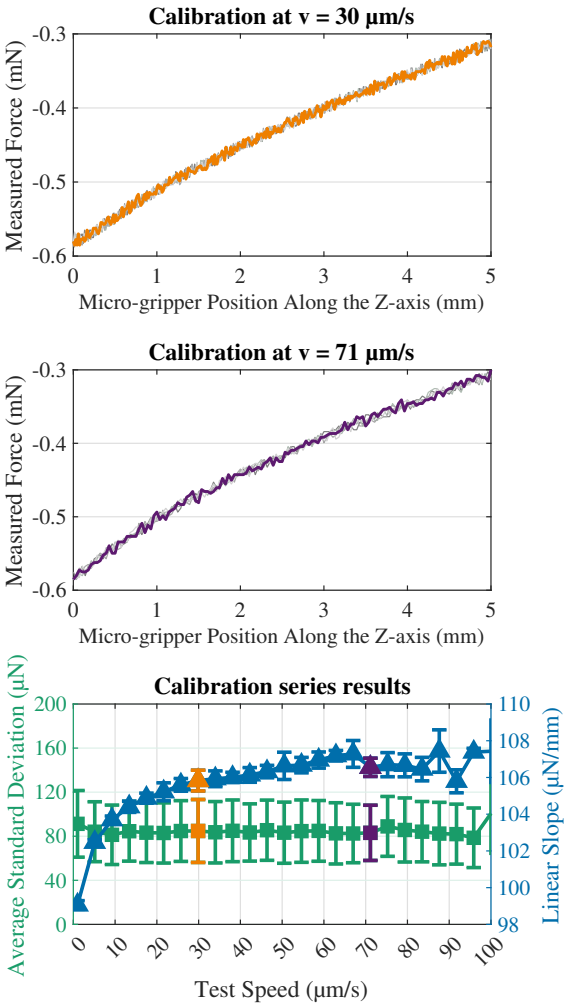

Fig. 6. Impact of calibration speed on the adopted force correction with a focus on two calibration tests results at speeds of 30 and 71 $\mu m/s$ showing 5 repetitions each (with only one highlighted for ease of reading).

E. Experimental protocol

1) Sample mounting: To mount the manually prepared fiber sample on the experimental setup, the micro-gripper is removed from its seat on the rail system and placed on an open surface for ease of manipulation. The elementary fiber that is partly separated from its parent bundle is grasped by the micro-gripper and both are then placed back on the experimental platform. The fiber bundle is visually centered along the axis of the gripping jaws before locking it in place using screws. A tension load is applied to the mounted bundle by the means of the manual positioning stage to remove any existing slack to avoid fiber bundle deflection during the peeling.

At this stage, adjustments are made to the sample position, viewed under the setup camera, so that the peeling zone - the meeting point of the elementary fiber and its parent bundle - is visible and in-focus. Based on the camera display, the peeling angle is set to 90° by adjusting the positions of the sample and the micro-gripper.

2) Peeling force reference: One important aspect of the peeling test preparation and its later data processing is having a specific reference point for the force measurement. The manipulation of the micro-gripper during the mounting of each sample, especially its removal and placement on its rail system that is directly attached to the force sensor, leads to the variation in the baseline of the peeling force measurement at the beginning of each individual peeling test.

To reliably define the reference point for a peeling test, the micro-gripper grasping the mounted elementary fiber is moved, using a manual precision positioning stage, to the closest point possible to the mounted bundle which is the limit stop of the positioning stage. At this point, the grasped elementary fiber is released from the micro-gripper hands ensuring thus that the latter experiences no load.

The movement of the micro-gripper to the limit stop of the positioning stage ensures protocol repeatability throughout all peeling tests, and the release of the elementary fiber eliminates any load exerted by the fiber on the micro-gripper due to any potential buckling of the fiber following this forward movement.

A two-minute idle state marks this step in the peeling force sensor output data and serves to determine the reference point during the data processing phase. The average value of the reference force obtained using this protocol is used to shift the measured peeling force. The result of this shift is the actual peeling force calculated via the following equation:

$$F_{peeling} = F_{measured} - F_{correction} + |F_{reference}| \quad (4)$$

Fig. 7 shows the steps of the implemented experimental protocol at the campaign level and at the individual peeling test level.

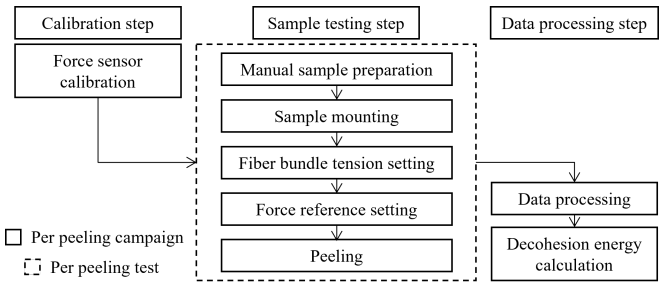

Fig. 7. Experimental protocol steps.

III. RESULTS & DISCUSSION

The peeling test data is processed and plotted against the peeling distance. The gathered data is rich in information, however, the force plot alone is not sufficient to form a complete image of the peeling process and the phenomena involved in it. Therefore, the peeling force plot is paired with the peeling video and the synchronization of the two correlates the observed peeling force with certain mechanisms taking place at various interesting points during the peeling. A peeling video is made available in the supplementary data of this paper.

A. Peeling force

Typical results for the tested plant fibers are presented in the graphs of Fig. 8 where the measured peeling force is plotted against the peeling distance for two different hemp varieties and one nettle.

The characteristic "stick-and-slip" behavior appears in the plot in both cases; the peeling force shows a cyclic behavior where it increases until a local threshold at which it experiences an instantaneous drop; this increased peeling force is the force needed for the decohesion initiation, and it is typically followed by a force drop until the fiber, now slack, becomes tensioned again. This particular peeling pattern is attributed to two observed decohesion mechanisms, discussed in detail in the next section, taking place during the peeling process. In the graph of the second hemp fiber, instances of the impact of the different peeling mechanisms on the measured peeling force are marked with the letters corresponding to the images of those mechanisms in Fig. 9.

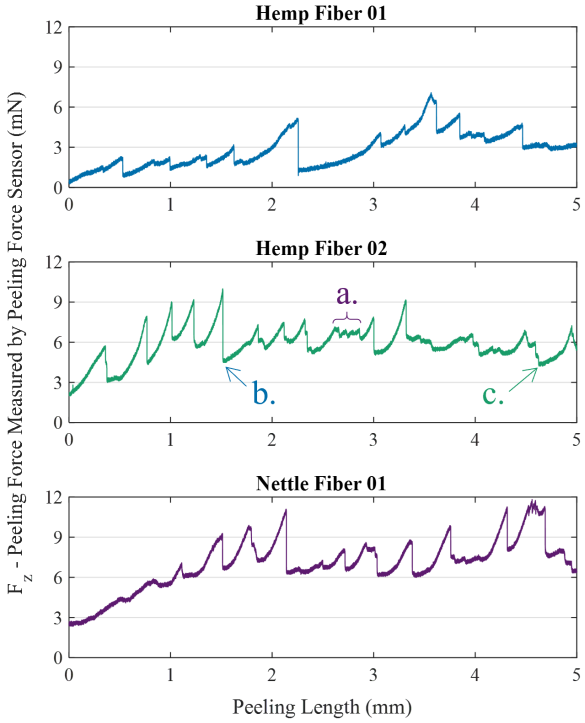

Fig. 8. Peeling force plots of 2 hemp fibers and 1 nettle fiber as a function of the peeling length with the peeling force profiles (a., b. and c.) of the different decohesion mechanisms referenced in Fig. 9 (a synchronized plot of the peeling force with the peeling video is available in the supplementary files for the article).

An order of magnitude for the peeling force of hemp fibers can be deducted from the tests. In the studied cases, the hemp fibers and nettle fibers necessitate an average force of $7.40 \pm 4.03\ mN$ and $7.40 \pm 4.17\ mN$, respectively, to be peeled off. The standard deviation of the peeling force in both cases is relatively high due to the different peeling mechanisms taking place, detailed in the following section. The adhesion constant, consisting in the normalized peeling force by the area of the contact surface between the peeled fiber and its parent bundle, falls in the range of $0.28 \pm 0.15\,mN/mm$ and $0.24 \pm 0.11\,mN/mm$ for hemp and nettle respectively. Table I offers a comparison between the interfacial adhesion force of the tested fibers and other objects at the micro-scale [4], [31].

B. Peeling mechanisms

A detailed inspection of the obtained graphs reveals firstly a non-null peel force baseline, as well as notable force drops following specific peaks. A closer analysis of these points correlates them to two main rupture mechanisms observed all throughout the nominal peeling process: the debonding of kink-bands and the peel-off of fiber-bridging areas.

	Peeling force (mN)	Adhesion constant (mN/mm)
Fish scales [31]	N/A	38.6 ± 9.8
Wood [4]	N/A	$[100,\ 300]$
Hemp fibers (this paper)	7.40 ± 4.03	0.28 ± 0.15
Nettle fibers (this paper)	7.40 ± 4.17	0.24 ± 0.11

TABLE I
EXPLOITATION OF INTERFACIAL ADHESION PEELING DATA MEASURED FOR THE FIRST TIME FOR HEMP AND NETTLE FIBERS, AS COMPARED WITH FISH SCALES AND WOOD.

The peeling force baseline characterizes the nominal peeling mechanism in which the peeling happens between the individual peeled fiber and its parent bundle and consists in tearing away the "adhesive" holding the fibers together (Fig. 9.a), this being mainly pectin. The observed peeling force peaks correspond to the kink-bands (Fig. 9.b) and fiber-bridging areas (Fig. 9.c) which require a significant amount of force for the crack initiation and the peeling due to their particular morphology.

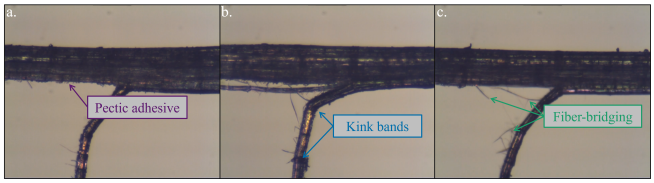

Fig. 9. Peeling mechanisms of the pectic adhesive layer between the elementary fiber walls (a.), the kink-bands (b.), and the fiber-bridging regions (c.) observed during a peeling test of a hemp fiber.

These mechanisms, introduced in Fig. 1, and governing the decohesion of plant fibers, are observed during the peeling tests using the setup camera. Fig. 9 showcases the three decohesion mechanisms as observed during the peeling test of a single fiber specimen. A video presenting the working principle of the experimental setup and showing a commented peeling video is available for viewing in the supplementary data to this paper.

IV. CONCLUSIONS

This work addresses the currently limited understanding of the magnitudes of forces involved in the intra-fiber adhesion and the testing methodologies regarding micro-scale peeling of elementary plant fibers. To the knowledge of the authors, no known experimental system has been previously identified capable of such peeling with minute force amplitudes (mN) and great displacements (mm). However, an experimental platform is successfully developed that allows for the gripping of all three ends of the plant fiber, the application of controlled tension, and the performance of peeling while maintaining a $90°$ angle. By integrating synchronized movements, the peeling process can be observed and analyzed under a microscope. A direct measurement of the interfacial adhesion forces is thus made possible.

Initial estimates of force magnitudes for natural fibers (mN) are obtained, indicating that an approximate force of a few mN is required to initiate peeling. The obtained results reveal comparable figures in terms of the adhesion energy of the plant fibers, tested using the presented experimental setup, with respect to other similar bio-materials at the micro-structural scale, such as the interfibrillar interfaces in wood [4].

Furthermore, various phenomena occurring in the plant fiber peeling process are identified and their prints on the peeling force profile highlighted. In addition to nominal peeling, kink-band and fiber-bridging-areas peeling are also encountered, giving the force profile observed during peeling its characteristic stick-and-slip appearance.

Based on this work, it is now possible to conduct micro-scale peeling tests on elementary plant fibers. An interesting future perspective would be the implementation of methods to improve the precision of contact area estimation. Additionally, the exploration of these techniques on other similar bio-based objects of interest, as well as the incorporation of multi-modal measurements, such as 3D geometry measurements, could further enhance understanding in this field.

ACKNOWLEDGMENT

The authors would like to thank Patrick Rougeot and Pierre Roux for their technical help in the design and manufacturing of the experimental platform, and Stefano Amaducci for providing the testing material for this study.

REFERENCES

[1] W. Li, R. Zhou, Y. Ouyang, Q. Guan, Y. Shen, E. Saiz, M. Li, and X. Hou, "Harnessing biomimicry for controlled adhesion on material surfaces," *Small*, p. 2401859, 2024.
[2] L. Mwaikambo, "Review of the history, properties and application of plant fibres," *African Journal of Science and Technology*, vol. 7, no. 2, p. 121, 2006.
[3] M. Weiss, J. Haufe, M. Carus, M. Brandão, S. Bringezu, B. Hermann, and M. K. Patel, "A review of the environmental impacts of biobased materials," *Journal of Industrial Ecology*, vol. 16, pp. S169–S181, 2012.
[4] F. Barthelat, Z. Yin, and M. J. Buehler, "Structure and mechanics of interfaces in biological materials," *Nature Reviews Materials*, vol. 1, no. 4, pp. 1–16, 2016.
[5] S. Pettersson, J. Engqvist, S. Hall, N. Toft, and H. Hallberg, "Peel testing of a packaging material laminate studied by in-situ x-ray tomography and cohesive zone modeling," *Int. J. of Adhesion and Adhesives*, vol. 95, p. 102428, 2019.
[6] D. Badler, R. Goltsberg, A. A. Ammar, and H. Kasem, "Experimental study of adhesion, friction, and peeling of biomimetic combined micro-mushroom and micro-spatulae textures," *Tribology Int.*, vol. 186, p. 108609, 2023.
[7] F. R. Leiro, S. Régnier, S. Haliyo, and M. Boudaoud, "A robotic strategy for in-plane center of rotation identification and control in atomic force microscopy," *IEEE Rob. and Autom. Let.*, vol. 9, no. 1, pp. 523–530, 2023.
[8] F. J. Schmied, C. Teichert, L. Kappel, U. Hirn, W. Bauer, and R. Schennach, "What holds paper together: Nanometre scale exploration of bonding between paper fibres," *Scientific reports*, vol. 3, no. 1, p. 2432, 2013.
[9] Y. Lei, C. Clévy, J.-Y. Rauch, and P. Lutz, "Large-workspace polyarticulated micro-structures based-on folded silica for tethered nanorobotics," *IEEE Rob. and Autom. Let.*, vol. 7, no. 1, pp. 88–95, 2021.
[10] H. Hussein, A. A. Bazroun, and H. Fariborzi, "Microrobotic leg with expanded planar workspace," *IEEE Rob. and Autom. Let.*, vol. 7, no. 3, pp. 5998–6004, 2022.
[11] G. Adam, M. Boudaoud, V. Reynaud, J. Agnus, D. J. Cappelleri, and C. Clévy, "An overview of microrobotic systems for microforce sensing," *Annual Review of Control, Robotics, and Autonomous Systems*, vol. 7, 2024.

[12] H. Zang, S. Pang, B. Zhu, H. Zhang, H. Li, S. Fatikow, and X. Zhang, "Development of a microforce sensor based on a fiber bragg grating used for micro-/nanomanipulation," *IEEE Trans. on Instrum. and Meas.*, vol. 72, pp. 1–10, 2023.

[13] G. Adam, G. Ulliac, C. Clevy, and D. J. Cappelleri, "3d printed vision-based micro-force sensors for microrobotic applications," *Journal of Micro and Bio Robotics*, vol. 18, no. 1, pp. 15–24, 2022.

[14] K. Feng, Q. Xu, and L. M. Tam, "Design and development of a dexterous bilateral robotic microinjection system based on haptic feedback," *IEEE Trans. on Autom. Sc. and Eng.*, vol. 20, no. 2, pp. 1452–1462, 2022.

[15] P. Rao, C. Pogue, Q. Peyron, E. Diller, and J. Burgner-Kahrs, "Modeling and analysis of tendon-driven continuum robots for rod-based locking," *IEEE Rob. and Autom. Let.*, vol. 8, no. 6, pp. 3126–3133, 2023.

[16] A. Awde, M. Boudaoud, M. Macioce, S. Régnier, and C. Clévy, "A microrobotic approach for the intuitive assembly of industrial electrooptical sensors based on closed-loop light feeling," *IEEE/ASME Trans. on Mech.*, vol. 27, no. 6, pp. 5462–5471, 2022.

[17] Q. Boyer, S. Voros, P. Roux, F. Marionnet, K. Rabenorosoa, and M. T. Chikhaoui, "On high performance control of concentric tube continuum robots through parsimonious calibration," *IEEE Rob. and Autom. Let.*, 2024.

[18] H. Bettahar, C. Clévy, N. Courjal, and P. Lutz, "Force-position photorobotic approach for the high-accurate micro-assembly of photonic devices," *IEEE Rob. and Autom. Let.*, vol. 5, no. 4, pp. 6396–6402, 2020.

[19] A. N. André, O. Lehmann, J. Govilas, G. J. Laurent, H. Saadana, P. Sandoz, V. Gauthier, A. Lefevre, A. Bolopion, J. Agnus, *et al.*, "Automating robotic micro-assembly of fluidic chips and single fiber compression tests based-on θ visual measurement with high-precision fiducial markers," *IEEE Trans. on Autom. Sc. and Eng.*, vol. 21, no. 1, pp. 353–366, 2022.

[20] Y. Han, A. Routray, J. O. Adeghate, R. A. MacLachlan, J. N. Martel, and C. N. Riviere, "Monocular vision-based retinal membrane peeling with a handheld robot," *J. of Medical Devices*, vol. 15, no. 3, p. 031014, 2021.

[21] S. Sunshine, M. Balicki, X. He, K. Olds, J. U. Kang, P. Gehlbach, R. Taylor, I. Iordachita, and J. T. Handa, "A force-sensing microsurgical instrument that detects forces below human tactile sensation," *Retina*, vol. 33, no. 1, pp. 200–206, 2013.

[22] B. Gonenc, P. Gehlbach, J. Handa, R. H. Taylor, and I. Iordachita, "Motorized force-sensing micro-forceps with tremor cancelling and controlled micro-vibrations for easier membrane peeling," in *5th IEEE RAS/EMBS Int. Conf. on Biomedical Robotics and Biomechatronics*, pp. 244–251, 2014.

[23] M. S. Magnusson, X. Zhang, and S. Östlund, "Experimental evaluation of the interfibre joint strength of papermaking fibres in terms of manufacturing parameters and in two different loading directions," *Experimental mechanics*, vol. 53, pp. 1621–1634, 2013.

[24] M. S. Magnusson, W. J. Fischer, S. Östlund, and U. Hirn, "Interfibre joint strength under peeling, shearing and tearing types of loading," *Adv Pulp Pap Res. Cambridge*, pp. 103–124, 2013.

[25] O. Grigoray, H. Wondraczek, S. Daus, K. Kühnöl, S. K. Latifi, P. Saketi, P. Fardim, P. Kallio, and T. Heinze, "Photocontrol of mechanical properties of pulp fibers and fiber-to-fiber bonds via self-assembled polysaccharide derivatives," *Macromolecular Materials and Engineering*, vol. 300, no. 3, pp. 277–282, 2015.

[26] P. Saketi, *Microrobotic platform with integrated force sensing microgrippers for characterization of fibrous materials: Case study on individual paper fibers*. PhD thesis, Tampere Univ. of Tech., 2015.

[27] A. Bourmaud, J. Beaugrand, D. U. Shah, V. Placet, and C. Baley, "Towards the design of high-performance plant fibre composites," *Progress in Materials Science*, vol. 97, pp. 347–408, 2018.

[28] E. Richely, A. Bourmaud, V. Placet, S. Guessasma, and J. Beaugrand, "A critical review of the ultrastructure, mechanics and modelling of flax fibres and their defects," *Progress in Materials Science*, vol. 124, p. 100851, 2022.

[29] V. Placet, C. François, A. Day, J. Beaugrand, and P. Ouagne, "Industrial hemp transformation for composite applications: Influence of processing parameters on the fibre properties," in *Advances in natural fibre composites*, pp. 13–25, Springer, 2018.

[30] K. Kendall, "Thin-film peeling-the elastic term," *Journal of Physics D: Applied Physics*, vol. 8, no. 13, p. 1449, 1975.

[31] A. K. Dastjerdi and F. Barthelat, "Teleost fish scales amongst the toughest collagenous materials," *J. of the mechanical behavior of biomedical materials*, vol. 52, pp. 95–107, 2015.